Journal of Natural Gas Science and Engineering 59 (2018) 274–286

Contents lists available at ScienceDirect

Journal of Natural Gas Science and Engineering

journal homepage: www.elsevier.com/locate/jngse

Analysis method of pulse decay tests for dual-porosity cores

Guofeng Han[a], Liang Sun[b,*], Yuewu Liu[a], Shangwen Zhou[b]

[a] Institute of Mechanics, Chinese Academy of Sciences, Beijing, 100190, China
[b] PetroChina Research Institute of Petroleum Exploration & Development, Beijing, 100083, China

ARTICLE INFO

Keywords:
Pulse decay test
Transient dual-porosity model
Pseudosteady-state dual-porosity model
Permeability

ABSTRACT

Homogeneous models are typically used to analyze the results of pulse-decay tests for low permeability cores. However, this poses a problem because some samples are dual-porosity media with microcracks/macropores and micropores. In this study, numerical simulations were conducted and the results showed that the pulse decay curves of the dual-porosity models are different from those for the homogeneous model. The results indicated that the volumes of the upstream and downstream vessels play an important role in identifying dual-porosity media and the early time and late time are mainly influenced by the storativity ratio and interporosity flow coefficient, respectively. A pressure derivative method was proposed in this work in order to identify dual-porosity media at the early time and distinguish the interporosity flow models. This method is applicable for vessel volumes within one-tenth to ten times the pore volume. The proposed method was verified against the experimental data of other researchers.

1. Introduction

Steady and transient methods are typically used to determine the permeability of rock cores. For low permeability rocks, the pulse decay method (which is a transient method) has become the mainstream method to determine the permeability of rock cores because it is much faster compared with the steady-state method. This method was proposed by Brace et al. (1968) to test the permeability of granite. The method was established based on the assumption that the elastic storativity of the core is negligible compared to those of the vessels. Since then, the pulse decay method has garnered much attention from other researchers because of its superior capability. Many analytical solutions were developed for various simplified conditions (Bourbie and Walls, 1982; Walder and Nur, 1986; Kwan et al., 1988). Hsieh et al. proposed a general analytical solution using a type curve matching method (Hsieh et al., 1981; Neuzil et al., 1981). Asymptotic solutions of pressures at early and late times were developed based on these analytical solutions and a number of linear fitting methods were proposed using these solutions. The effects of vessel volume, pressure, and core parameters have also been investigated and various methods were proposed to optimize the equipment parameters, accelerate test speed, and improve measurement accuracy (Chen and Stagg, 1984; Jones, 1997). All of these analysis methods are based on the homogeneous model.

Because shale gas reservoir with ultra-low permeability has become a popular research area in petroleum engineering, much effort has been carried out in this area in recent years. The pulse decay method have been also widely used to test the permeability of shale cores (Heller et al., 2014; Metwally and Sondergeld, 2011; Alnoaimi and Kovscek, 2013). Several new methods of analysis were proposed while experimental techniques were improved based on the characteristics of shale (Cui et al., 2009; Civan et al., 2011, 2012; Lorinczi et al., 2014; Pan et al., 2015). However, a few experimental studies have shown that the homogeneous model is not always applicable to analyze the permeability of rock cores, particularly shale cores (Clarkson and Bustin, 1999; Yuan et al., 2014; Alnoaimi et al., 2016) and therefore, multimedia models were also proposed for shale rocks. These models consider microcracks/macropores and micropores in the matrix, where these features are treated as dual-porosity media (Hudson, 2011; Dehghanpour and Shirdel, 2011). Both coal and shale consist of multiscale pores and fractures and their cores are characteristic of dual-porosity media. The pulse decay method is typically used to determine the permeability of coal and shale cores. Therefore, studies on analysis methods of pulse decay tests for dual-porosity cores have important implications for the development of coalbed methane and shale gas.

A few studies have been carried out over the years concerning pulse decay test for dual-porosity media. Numerical and experimental investigations have shown that the flow characteristics are different for dual-porosity media compared to those for homogeneous media when the cores contain penetrating cracks or thin alternating high and low permeability layers (Kamath et al., 1990; Liu et al., 2016; Jia et al.,

* Corresponding author.
E-mail address: sunliang0315@163.com (L. Sun).

https://doi.org/10.1016/j.jngse.2018.09.006
Received 26 April 2018; Received in revised form 16 August 2018; Accepted 12 September 2018
Available online 15 September 2018

2017). A few simplified models have been proposed to analyze the results obtained from pulse decay tests of such cores (Ning et al., 1993; Cronin, 2014; Liu et al., 2016). In these studies, the researchers merely used an approximate formula to analyze partial test results. While these simplified models are suitable to analyze the permeability of cores with a few microcracks or alternating high and low permeability layers, they are not suitable in cases where dense microcracks are present. Bajaalah (2009) studied dual-porosity models for pulse decay tests, in which their test is a two-dimensional flow in the radial plane of the cylindrical sample, but the conventional test method is a one-dimensional flow along the axial direction. In general, there is currently no analysis method of conventional pulse decay tests for dual-porosity cores to obtain all the parameters of dual-porosity models. So, it is necessary to develop an improved method to analyze the results obtained from conventional pulse decay tests for dual-porosity media.

In this paper, the analysis method of conventional pulse decay tests for dual-porosity cores is studied. First, the finite difference method is used to analyze the sensitivity of the relevant parameters of the dual-porosity models. Then a pressure derivative analysis method was proposed. Unlike conventional methods, the pressure derivative method facilitates in distinguishing dual-porosity and homogeneous media based on the early time pressure derivatives as well as identify pseudosteady-state and transient interporosity flow models based on the late time data. Finally, the proposed method is verified against the experimental results of other researchers.

2. Pulse decay test method

2.1. Experimental setup for pulse decay tests

The schematic of a typical experimental setup used for pulse decay tests is shown in Fig. 1 (Jones, 1997). The main components of the experimental setup comprise the upstream vessel, downstream vessel, and core holder. The rock sample is encased within a rubber sleeve in the core holder. The confining pressure can be applied to the sample from outside the rubber sleeve without interfering with the pore pressure. One end is connected to the upstream vessel whereas the other end is connected to the downstream vessel. The confining pressure is applied prior to the test and following this, an initial pressure is applied to the upstream vessel, downstream vessel, and pore space of the sample until all of the pressures reach an equilibrium. Next, Valve 1 (Fig. 1) is turned off, cutting off connection between the upstream vessel and core holder. The pressure of the upstream vessel is then increased to a value typically less than 10% of the initial pressure. Valve 1 is then turned on, creating a pressure pulse in the core holder. The fluid flows from the upstream vessel to the downstream vessel through the sample. Consequently, the upstream vessel pressure decreases and the downstream vessel pressure increases until these pressures reach an equilibrium. The upstream and downstream vessel pressures and the difference between these pressures are recorded as a function of time. The variations of these pressures are dependent on the permeability of the sample. The permeability can be determined by analyzing the pressure-time histories. In practice, the pulse-decay test is not only used

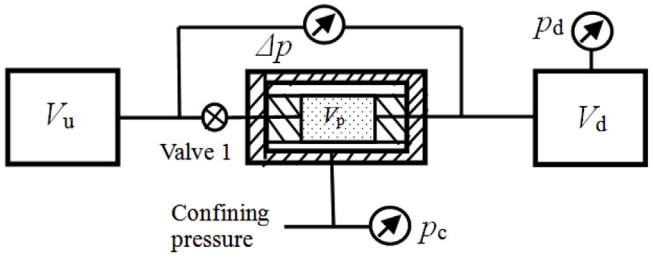

Fig. 1. Schematic of a typical experimental setup used for pulse decay tests (after Jones, 1997).

to determine the permeability of homogeneous media, but also dual-porosity media. The analysis method proposed in this work is also based on the pulse decay test method shown in Fig. 1.

2.2. Analysis method for homogeneous media

The dimensionless governing equation for pulse decay tests in order to determine the permeability of a homogeneous medium is given by (Dicker and Smits, 1988):

$$\frac{\partial p_D}{\partial t_D} = \frac{\partial p_D^2}{\partial x_D^2} \tag{1}$$

The dimensionless initial conditions are:

$$p_D(x_D, 0) = 0, 0 < x_D < 1\ p_D(0,0) = 1 \tag{2}$$

The dimensionless boundary conditions are:

$$p_D(0, t_D) = p_{uD}(t_D),\ t_D \geq 0 \tag{3}$$

$$p_D(1, t_D) = p_{dD}(t_D),\ t_D \geq 0 \tag{4}$$

$$\frac{dp_{uD}}{dt_D} = A_u \left.\frac{\partial p_D}{\partial x_D}\right|_{x_D=0},\ t_D > 0 \tag{5}$$

$$\frac{dp_{dD}}{dt_D} = -A_d \left.\frac{\partial p_D}{\partial x_D}\right|_{x_D=1},\ t_D > 0 \tag{6}$$

The dimensionless variables are defined as:

$$t_D = \frac{kt}{\mu\phi c_t L^2},\ x_D = \frac{x}{L},\ p_D = \frac{p(t) - p_d(0)}{p_u(0) - p_d(0)},\ A_u = \frac{V_p c_t}{V_u(c_L + c_{V_u})},\ A_d = \frac{V_p c_t}{V_d(c_L + c_{V_d})} \tag{7}$$

where p is pressure (Pa), the subscripts f and m represent macropores and micropores, respectively, the subscripts u and d represent the upstream and downstream vessels, respectively, t is time (s), x is the axial coordinate along the length of the sample beginning from the upstream vessel (m), and L is the length of the sample (m). V_u,V_d, and V_p denote the volumes of the upstream vessel, downstream vessel, and core pore, respectively (m^3), c_L is the compressibility of the fluid used in the pulse-decay test (Pa^{-1}), c_t is the total compressibility of the core (Pa^{-1}), c_{Vu} and c_{Vd} represent the compressibility of the upstream and downstream vessels, respectively (Pa^{-1}), ϕ is porosity (%), k is permeability (m^2), and μ is the fluid viscosity (Pa·s).

If the pressure pulse is very small, the dimensionless differential pressure becomes an exponential function of time at the late stage (Jones, 1997):

$$\ln(\Delta p_D) = \ln(f_0) + s_1 t \tag{8}$$

where f_0 is a constant and s_1 is given by

$$s_1 = -\frac{k\theta_1^2}{\mu\phi c_t L^2} \tag{9}$$

It shall be noted that θ_1 is the first root of the following equation:

$$\tan\theta = \frac{(A_u + A_d)\theta}{\theta^2 - A_u A_d} \tag{10}$$

The slope s_1 can be obtained by linearly fitting $\ln(\Delta p_D)$-t with the pulse decay test data at the late stage. The permeability of the cores can then be determined by using equation (9).

3. Mathematical models for dual-porosity media

In this work, for convenience, fractures refer to relatively bigger pores and microcracks whereas matrices refer to relatively smaller pores. The permeability of dual-porosity media can be represented by

dual-porosity models, which are presented in Appendix A. The dimensionless governing equations of pseudosteady-state dual-porosity models for pulse decay tests are given by:

$$\omega\frac{\partial p_{fD}}{\partial t_D} = \frac{\partial p_{fD}^2}{\partial x_D^2} + \lambda_D(p_{mD} - p_{fD}) \tag{11}$$

$$-\lambda_D(p_{mD} - p_{fD}) = (1-\omega)\frac{\partial p_{mD}}{\partial t_D} \tag{12}$$

The dimensionless variables are defined as follows: $t_D = \frac{k_f t}{\mu[(\phi c_t)_f + (\phi c_t)_m]L^2}$, $p_{fD} = \frac{p_f(t) - p_d(0)}{p_u(0) - p_d(0)}$, $A_u = \frac{V_p[(\phi c_t)_f + (\phi c_t)_m]}{\phi V_u(c_L + c_{Vu})}$, $A_d = \frac{V_p[(\phi c_t)_f + (\phi c_t)_m]}{\phi V_d(c_L + c_{Vd})}$, storativity ratio $\omega = \frac{(\phi c_t)_f}{(\phi c_t)_f + (\phi c_t)_m}$ interporosity flow coefficient

$$\lambda_D = \frac{\alpha k_m L^2}{k_f} \tag{13}$$

where the subscripts f and m denote macropores and micropores respectively, and α is the shape factor.

The dimensionless initial conditions are:

$$p_{fD}(x_D, 0) = p_{mD}(x_D, 0) = 0, 0 < x_D < 1\ p_{fD}(0,0) = 1 \tag{14}$$

The dimensionless boundary conditions of the pseudosteady-state dual-porosity model can be obtained if the dimensionless variable p_D in equations (3)–(6) is replaced by p_{fD}.

Assuming that the core matrix is a slab, the dimensionless governing equations for the transient dual-porosity model are:

$$\omega\frac{\partial p_{fD}}{\partial t_D} = \frac{\partial}{\partial x_D}\left(\frac{\partial p_{fD}}{\partial x_D}\right) + \frac{\lambda_D}{6}\frac{\partial p_{mD}}{\partial z_D}\bigg|_{z_D=0} \tag{15}$$

$$\frac{12(1-\omega)}{\lambda_D}\frac{\partial p_{mD}}{\partial t_D} = \frac{\partial^2 p_{mD}}{\partial z_D^2} \tag{16}$$

The following dimensionless variable is added to the list of the dimensionless variables defined in (13):

$$z_D = \frac{z}{h_m} \tag{17}$$

where h_m is the thickness of the slab matrix and z is the matrix coordinate.

The dimensionless initial conditions are:

$$p_{fD}(x_D, 0) = p_{mD}(x_D, z_D, 0) = 0,\ 0 < x_D < 10 \le z_D \le 1/2\ p_{fD}(0,0) = 1 \tag{18}$$

In addition to the boundary conditions used in the pseudosteady-state model, the transient dual-porosity model needs to fulfill the following boundary conditions:

$$\frac{\partial p_{mD}}{\partial z_D}\bigg|_{z_D=1/2} = 0 \tag{19}$$

$$p_{mD}|_{z_D=0} = p_{fD} \tag{20}$$

The pseudosteady-state and transient dual-porosity models can be numerically solved and the details are given in Appendices B and C.

4. Simulation results and analysis

4.1. Comparison between dual-porosity and homogeneous models

Fig. 2 shows the upstream and downstream vessel pressure curves for the pseudosteady-state and transient dual-porosity models and homogeneous model. The variable p_D is used for both the upstream and downstream vessel pressures. It can be seen that the shapes of the pressure curves at early time ($t_D > 10$) are similar for the dual-porosity and homogeneous models. It is apparent that the upstream and downstream vessel pressures approach one another quickly. The upstream vessel pressures for the pseudosteady-state and transient dual-porosity models decrease at a slower rate than those for the homogeneous model whereas the downstream vessel pressures of the dual-porosity models show the opposite trend. A pressure plateau appears ($10 < t_D < 10^2$) after the pressures reach an equilibrium. The pressures of the homogeneous model remain stable but the pressures of the dual-porosity models decrease together ($10^2 < t_D < 10^5$) to the same final pressure $A_d/(A_u + A_d + A_uA_d)$ of the homogeneous model. The differences between the dual-porosity and homogeneous models are likely because the fluid flows faster in the fractures compared with that in the matrix and more time is required for the pressure in the matrix to achieve equilibrium. Using the same values for A_u and A_d, the upstream and downstream vessel pressures for different models eventually reach the same value, in accordance with the law of conservation of mass. Based on the parameters in Fig. 1, the pressures of the dual-porosity models are almost equal at the early and last stages and the difference between the pressure curves becomes obvious from the first plateau to the second one. The shapes of the pulse decay curves are very similar to that of a core with several penetrating fractures or alternating high and low permeability layers. After the upstream and downstream pressures converge into a plateau, they reduce together until the final equilibrium (Ning et al., 1993; Cronin, 2014; Liu et al., 2016).

4.2. Effect of vessel volumes

Fig. 3 shows the effect of the upstream and downstream vessel volumes on the pressure curves. It shall be highlighted that the all of the pressure curves of the pseudosteady-state and transient dual-porosity models have the same storativity ratio and interporosity flow coefficient. It can be observed that the larger the vessel volume, the slower the pressure change and the higher the plateau. For different values of A_u and A_d, the first pressure plateaus (for $A_u = A_d = 1.0$, $2 < t_D < 30$) are relatively close. In general, the difference in the pressure curves between the dual-porosity and homogeneous models decrease with an increase in the upstream and downstream vessel volumes. In other words, it is difficult to distinguish between dual-porosity and homogeneous media based on the pressure curves if the upstream and downstream vessel volumes are ten times larger than that of the core pore.

4.3. Effect of storativity ratio

Fig. 4 shows the effect of storativity ratio on the pressure curves. It can be seen that the larger the storativity ratio, the faster the upstream vessel pressure changes and the slower the downstream vessel pressure changes. The height of the first pressure plateau ($8 < t_D < 10^3$) decreases as the storativity ratio increases because more fluid stays within the fractures for large storativity ratios. The analytical pressure of the first plateau is $A_d/(A_u + A_d + A_uA_d\omega)$ if the flux transporting into the matrix is negligible. Thus, the first pressure plateau approaches $A_d/(A_u + A_d)$ when the storativity ratio decreases to zero. Based on the definition of the storativity ratio, it can be deduced that the height of the first pressure plateau increases as the matrix porosity increases whereas it decreases as the fracture porosity increases.

4.4. Effect of interporosity flow coefficient

Fig. 5 shows the effect of interporosity flow coefficient on the pressure curves. It is obvious that the interporosity flow coefficient influences the duration of the first pressure plateau (for $\lambda = 10^{-5}$, $8 < t_D < 5 \times 10^2$). The larger the interporosity flow coefficient, the earlier the pressure drops from the first to the second plateau (for $\lambda = 10^{-5}$, $t_D > 4 \times 10^5$). This is because a larger interporosity flow coefficient indicates that fluid flows faster from the fracture to the matrix. The behavior of the transient interporosity flow model is similar

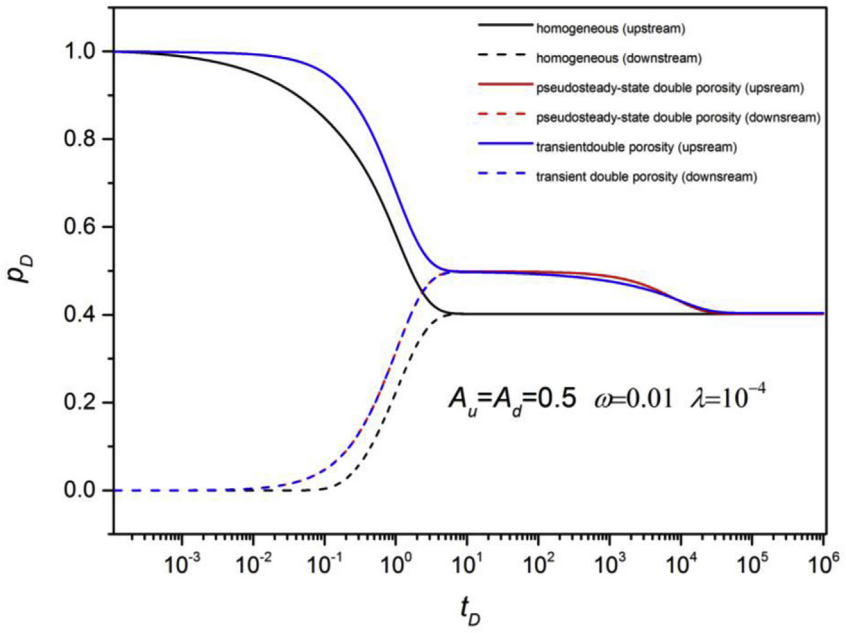

Fig. 2. Comparison of the upstream and downstream vessel pressures between the dual-porosity and homogeneous models.

to that of the pseudosteady-state model, except that the pressure of the former model drops slightly faster than that of the latter model. Based on the definition of the interporosity flow coefficient, it can be deduced that the duration of the first plateau increases with the fracture permeability whereas it decreases with the matrix permeability. When $\lambda = 0.1$, the pressure curves are very similar to the results of Alnoaimi et al. (2016), who observed that the upstream and downstream pressures decreased after convergence, which they called the "flowback phenomenon". This phenomenon is caused by the flow from the fracture into the matrix after the upstream and downstream pressures converge.

4.5. Comparison of permeability

The slope of the $\ln(\Delta p_D) - t_D$ curve is conventionally used to determine the permeability of rock cores based on the results obtained from pulse decay tests. Intuitively, for a dual-porosity medium, the fracture permeability is determined by the slope of the $\ln(\Delta p_D) - t_D$ curve at the early stage. However, this is not always the case. The permeability and other parameters need to be provided in order to perform numerical simulations using the finite difference method, producing the synthetic pulse-decay curve. The permeability is then determined from the synthetic pulse decay curve using semi-logarithmic linear analysis. The permeability provided for the numerical

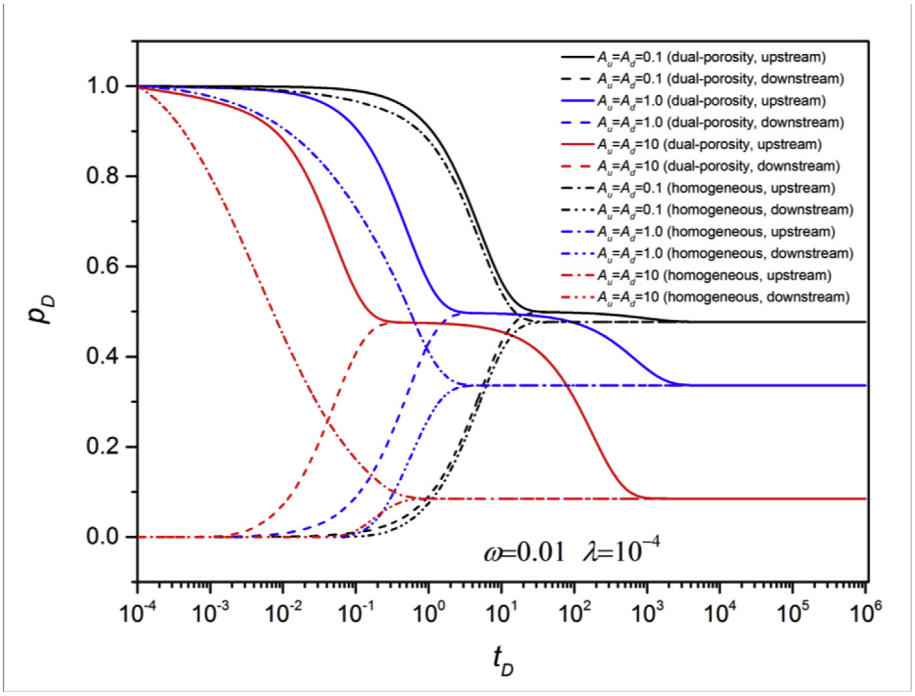

Fig. 3. Effect of the upstream and downstream vessel volumes on the pressure curves.

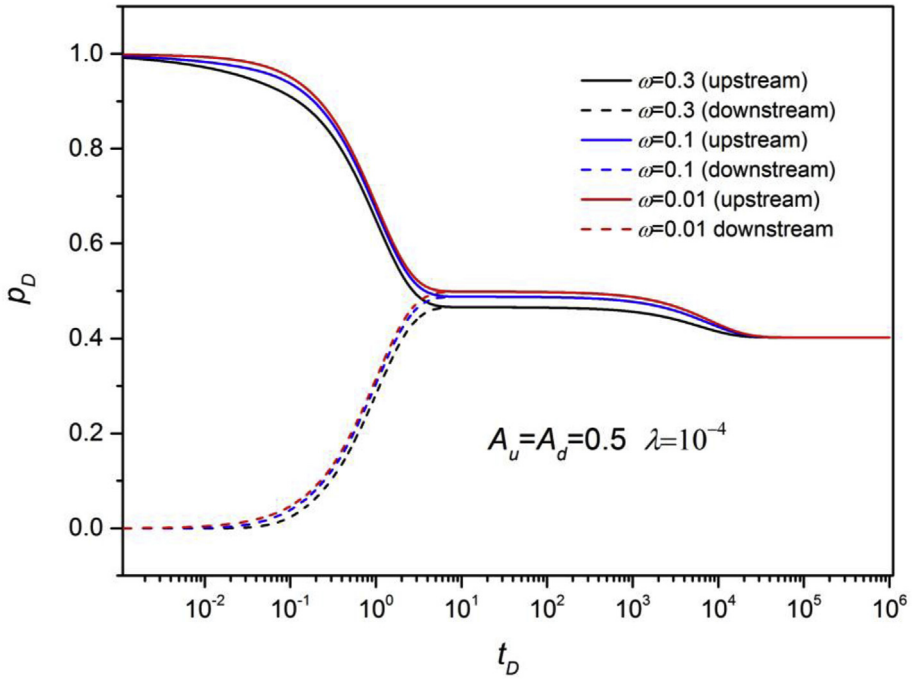

Fig. 4. Effect of storativity ratio on the pressure curves.

simulations is called the actual permeability. Fig. 6 shows the errors of the permeability obtained by applying semi-logarithmic linear analysis on the actual fracture permeability. It can be seen that the permeability error dramatically increases with a decrease in the vessel volumes and it slightly increases with a decrease in the storativity ratio. If the vessel volumes are ten times larger than the pore volume, then both permeabilities will be very close. If $A_u = A_d < 0.1$, the permeability difference is less than 2%. Analysis on the interporosity flow coefficient shows that its effect is negligible and the results of the transient dial-porosity model show very good agreement with those of the pseudosteady-state dual-porosity models.

5. Proposed analysis method for dual-porosity media

Dual-porosity media cannot be distinguished intuitively based on pressure curves at the early stage because the pressure curves for dual-porosity models are quite similar to those for the homogeneous model. The pulse decay test is usually stopped when the pressures are equal and the permeability of the homogeneous medium is then determined based on this pressure curve. In practice, the pulse-decay test is usually stopped when the permeabilities obtained from a segment of the data are almost constant. These pressure curves are not truncated properly and the curves would have been dual-porosity curves if the pulse-decay

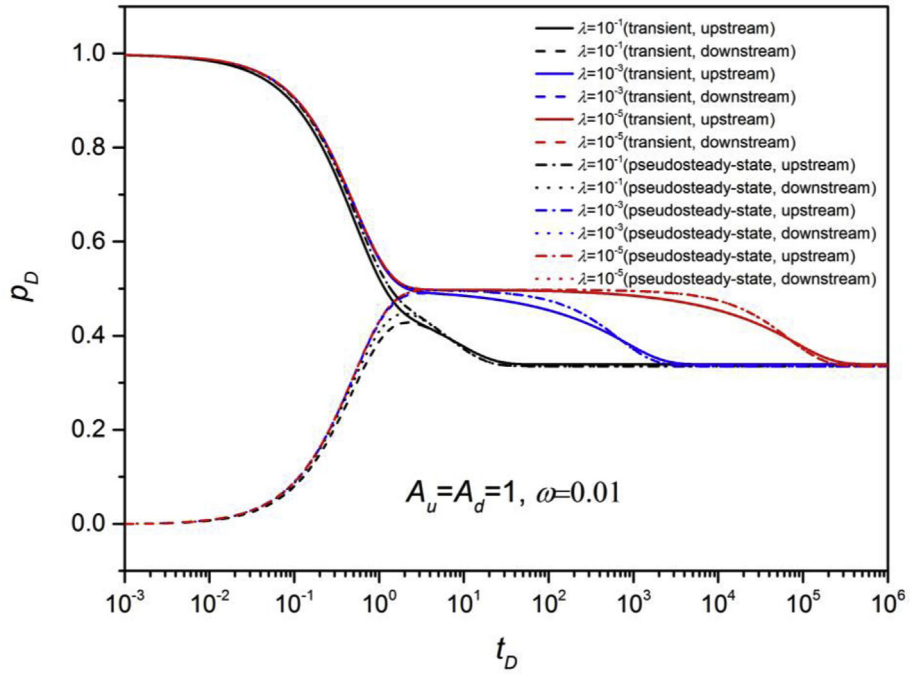

Fig. 5. Effect of interporosity flow coefficient on the pressure curves.

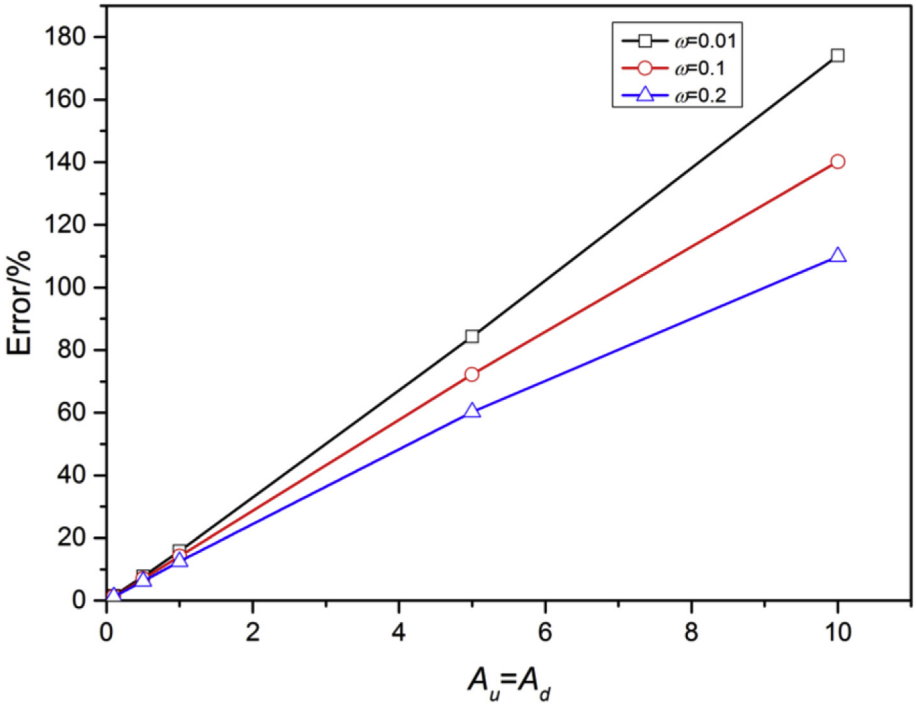

Fig. 6. Error of macropore permeability obtained from semi-logarithmic linear analysis.

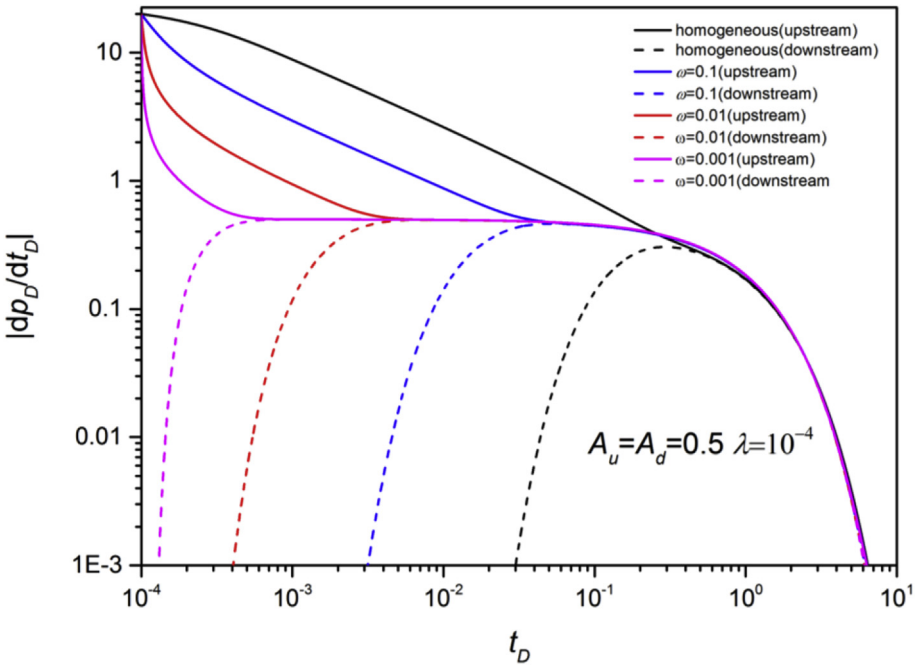

Fig. 7. Pressure derivative curves of the dual-porosity models at the early stage.

test is continued until pressure equilibrium is achieved between the fracture and matrix. Therefore, the pressure derivative-time curve was proposed in this study to identify and quantify the dual-porosity media. Even though the pressure derivative method is commonly used for well test analysis, it has not been used to analyze the results of pulse decay tests. Figs. 7–10 show the pressure derivative curves for the pseudos-teady-state and transient dual-porosity models. It shall be noted that the term “pressure derivative” refers to the absolute value of the pressure derivative with respect to time.

5.1. Homogeneous and dual-porosity models

Fig. 7 shows that there are plateaus in the pressure derivative curves for the dual-porosity models (for $\omega = 0.01$, $4 \times 10^{-3} < t_D < 0.1$) whereas there is no plateau in the pressure derivative curves for the homogeneous model. The smaller the storativity ratio, the earlier the onset of the pressure derivative plateau and the longer the plateau lasts. Therefore, dual-porosity media can be identified based on the early behaviors of the pressure derivative curves. In other words, the pulse decay test must be carried until the fracture and matrix pressures achieve equilibrium for cores when there is a plateau on the pressure

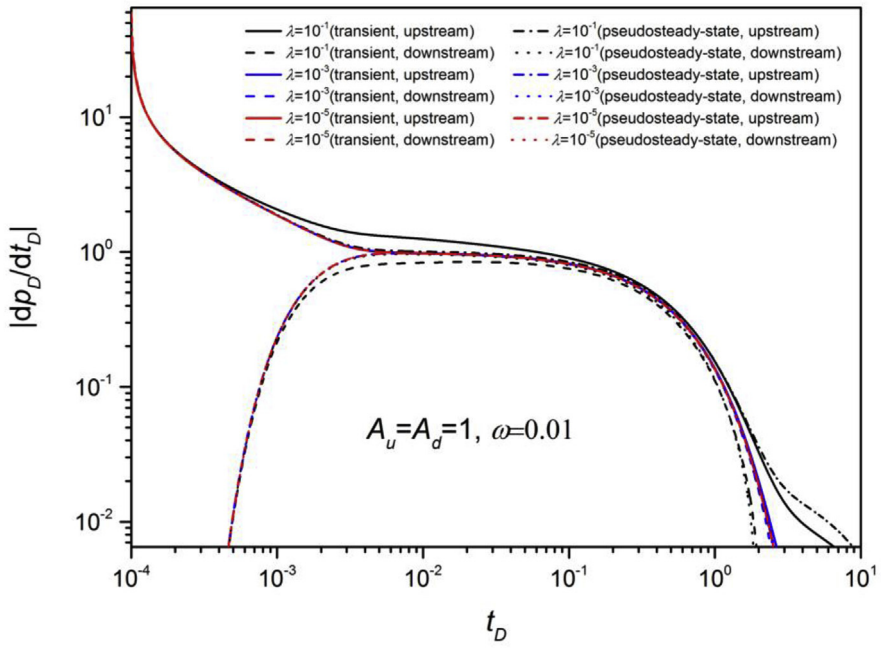

Fig. 8. Effect of interporosity flow coefficient on the pressure derivative curves at the early stage.

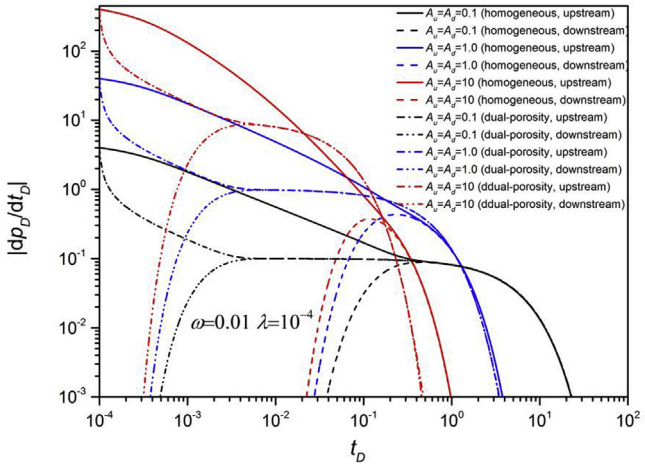

Fig. 9. Effect of the upstream and downstream vessel volumes on the pressure derivative curves at the early stage.

derivative curve. In addition, the pressure derivative curves are more sensitive to the storativity ratio compared to pressure curves.

Fig. 8 shows the effect of interporosity flow coefficient on the pressure derivative curves. It can be seen that an interporosity flow coefficient less than 10^{-3} barely affects the pressure derivative curves at the early stage. However, an interporosity flow coefficients greater than 0.1 causes the pressure derivative curves to separate slightly at the plateau, especially for the pseudosteady-state dual-porosity model. The slopes of the downstream pressure derivative curves are less steep than those for the upstream pressure derivative curves.

Fig. 9 shows the effect of the upstream and downstream vessel volumes on the pressure derivative curves at the early stage. In general, the larger the vessel volume, the longer and smaller the pressure derivative plateau (for $A_u = A_d = 1.0$, $4 \times 10^{-3} < t_D < 0.1$). When $A_u = A_d > 10$, the plateau is not very obvious and the pressure derivative curves of the dual-porosity models do not coincide with those of the homogeneous model. Based on the effects of the vessel volumes on the pressure curves and pressure derivative curves, it can be deduced that pressure derivative method is applicable if the volumes of the upstream and downstream vessels are within one-tenth to ten times the volume of the core pores. If the vessel volumes are more than ten times the pore volume, a plateau appears in the pressure derivative curves of the homogeneous model, rendering it difficult to distinguish between the pressure curves of the dual-porosity models and homogeneous model. In addition, there is a significance increase in the test duration. Likewise, if the vessel volumes are less than one-tenth the pore volume, the plateau of the pressure derivative curve is not apparent and therefore, it is not possible to distinguish between the dual-porosity and homogeneous models at the early stage.

5.2. Pseudosteady-state and transient interporosity flow models

There are two types of interporosity flow models based on the differences in the permeability and interfacial states between the matrix and fracture: (1) pseudo-steady state and (2) transient interporosity flow models. It can be seen from Fig. 5 that the first pressure plateau to the second pressure plateau is similar for the pressure curves of these models obtained from pulse decay tests and thus, these models cannot be distinguished from one another. Fig. 10 shows the pressure derivative curves during the transition from the first pressure plateau to the second pressure plateau. Indeed, the characteristics of transient and pseudosteady-state dual-porosity models are different. The pressure derivative curves of the pseudosteady-state model have a plateau (for $\lambda = 10^{-4}$, $20 < t_D < 2 \times 10^3$) whereas the pressure derivative curves of the transient model have a section of slant parallel lines for different interporosity flow coefficients. The larger the interporosity flow coefficient, the higher the pressure derivative plateau and the higher the slant line. Therefore, the pressure derivative curves at the late stage can be used as to identify the type of interporosity flow model. If this segment of the pressure derivative curve is a horizontal line, it can be deduced that the model is a pseudosteady-state interporosity flow model. In contrast, if the segment is an inclined straight line, the model is a transient interporosity flow model.

It shall be highlighted that log-log plots (plots where both axes are in the logarithmic scale) are used for Figs. 7–10. Log-log plots are

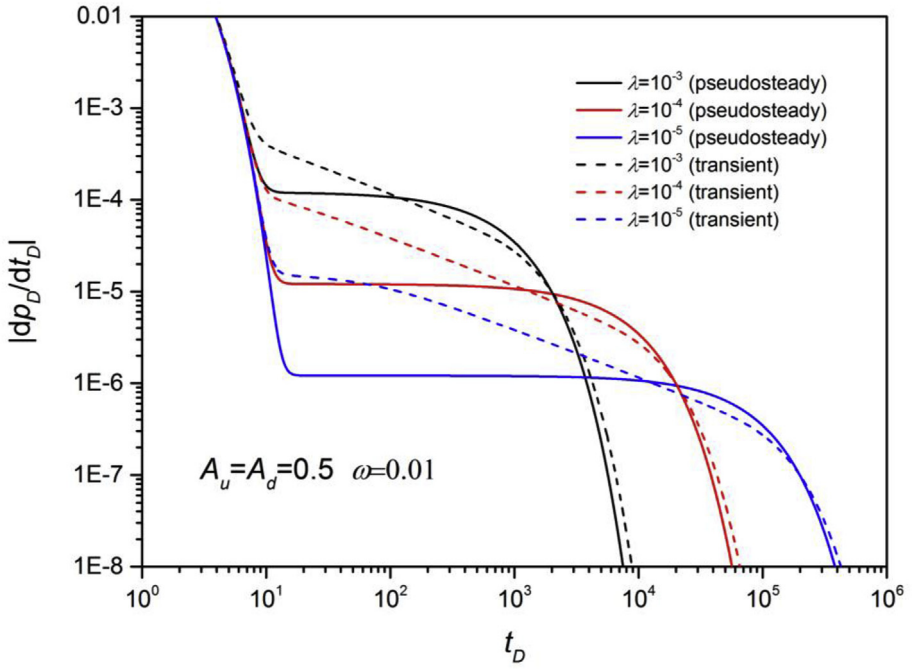

Fig. 10. Pressure derivative curves of the pseudosteady-state and transient dual-porosity models at the late stage.

widely used in well test analysis. Hence, the curves of the dimensionless and dimensional variables have the same shapes. Based on the aforementioned analysis, the pressure derivative curves can be used to choose the most appropriate model for the rock sample. The characteristics of a dual-porosity medium can be obtained by fitting both the pressure and pressure derivative curves in order to obtain more precise results, rather than fitting only pressure curves. It can be seen that the storativity ratio is primarily determined by the early-time data whereas the interporosity flow coefficient is mainly determined by the late-time data.

6. Discussion

The experimental results of Cronin (2014) and Alnoaimi et al. (2016) were used to verify the applicability of the pressure derivative method proposed in this study. Cronin (2014) performed pulse-decay tests on samples of Barnett Shale composed of two different property layers. Argon was used in the pulse decay tests. The properties of the samples and test settings are presented in Table 1. The simulation results obtained in this study were compared with the experimental data of Cronin (2014), as shown in Fig. 11 and Table 2. The transient interporosity flow model was used for the simulations. It can be seen from Fig. 11 that there is very good agreement in the dimensionless pressure and pressure derivative curves between the transient interporosity flow model and experimental results of Cronin (2014). In addition, it can be seen from Table 2 that the permeability obtained from simulations is very close to the permeability obtained by Cronin (2014). However, the storativity ratio obtained from simulations is lower than the value obtained by Cronin (2014). This is likely because Cronin (2014) assumed that the gas does not flow into the low permeability layers when the upstream and downstream pressures converge. Based on the results, it can be deduced that the transient interporosity flow model is suitable to determine the permeability of rock cores with alternating high and low permeability layers.

Table 1
Properties of the samples and settings used in the pulse-decay tests.

Parameters	Value		Unit
	Case 1 (Cronin, 2014)	Case 2 (Alnoaimi et al., 2016)	
Sample volume	19.85	25.51	cm^3
Porosity	6.9	5.6	%
Length	1.746	5.20[a]	cm
Downstream vessel pressure	950	228.09	psi
Upstream vessel pressure	1078	621.49	psi
Temperature	30	28	°C

[a] The sample diameter is assumed to be 2.5 cm, which is usually used in the literature.

For a given rock sample, upstream vessel pressure, and downstream vessel pressure, the fracture permeability can be determined by fitting the first plateau of the pressure derivative curve because this segment is related only to the fracture permeability. The storativity ratio can be determined from the starting time of this pressure derivative plateau. The interporosity flow coefficient can then be obtained by fitting the pressure derivatives during the interporosity flow stage. Finally, the fracture permeability, storativity ratio, and interporosity flow coefficient determined previously can be used to fit the pressure and pressure derivative histories. Due to the inaccuracy of identification and division of the flow regimes on pressure derivative curves, these parameters require a slight adjustment in order to improve the fitting of the histories.

Alnoaimi et al. (2016) used helium in their pulse decay tests. The properties of the samples and experimental settings are presented in Table 1. The simulation results obtained from the transient interporosity flow model were compared with the experimental results of Alnoaimi et al. (2016), as shown in Fig. 12 and Table 2. In general, there is very good agreement in the fracture permeability and storativity ratio obtained from simulations with those obtained by Alnoaimi et al. (2016). Due to the lack of early-time data in this case, the data could not be fitted according to the method used for Cronin (2014). When a pressure derivative is transformed into a dimensionless value, the fracture permeability determines the slope of the interporosity flow stage and its time coordinate position; the value of the interporosity flow coefficient determines its pressure derivative coordinate position of the interporosity flow stage. Therefore they can be uniquely determined by the pressure derivative fitting. Hence, the pressure

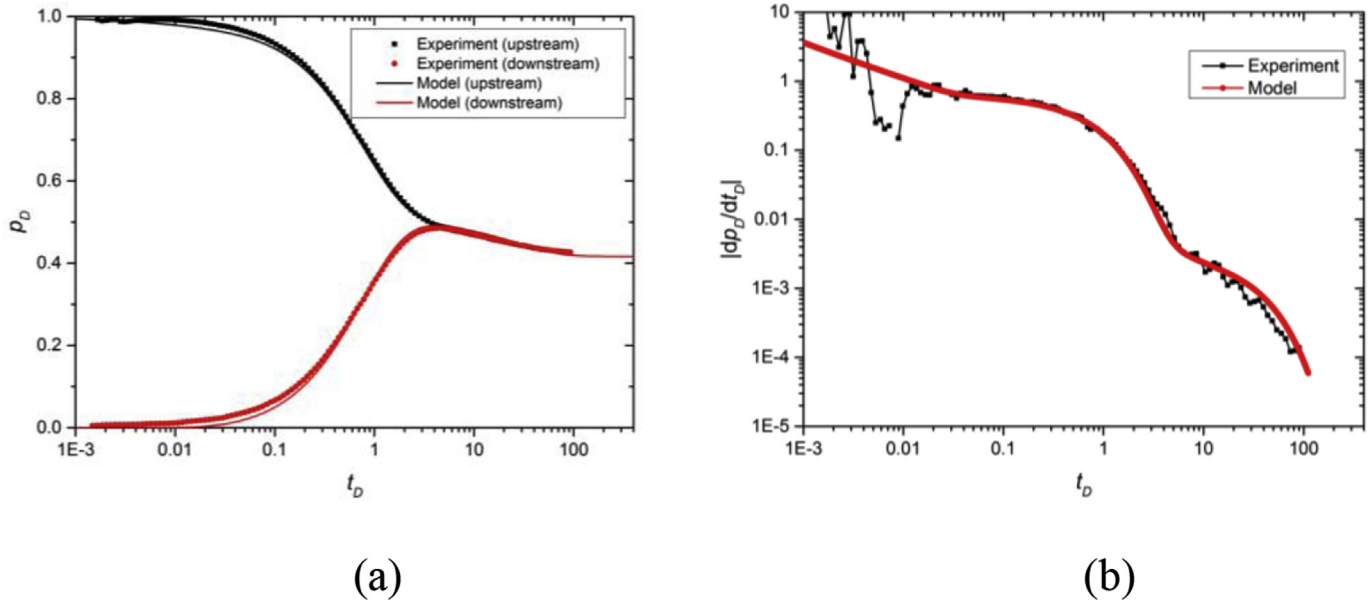

Fig. 11. Comparison between the simulation results and experimental data of Cronin (2014) for (a) pressure histories and (b) pressure derivative histories (from Cronin, 2014, Figure 2.5).

Table 2
Comparison between the simulation results obtained in this study and those of Cronin (201) and Alnoaimi et al. (2016).

Parameters	Case 1		Case 2		Unit
	Experimental results (Cronin, 2014)	Simulation results	Experimental results (Alnoaimi et al., 2016)	Simulation results	
k_f	0.092	0.11	1.75	1.50	μD
ω	0.48[a]	0.11	0.95[a]	0.92	–
λ	–	3.1×10^{-2}	–	2.0×10^{-3}	–

[a] Because the gas compressibility is significantly higher than the pore compressibility, the storativity ratio is almost the same as the rate of porosities.

derivatives at $t_D < 100$ (Fig. 12) were fitted to obtain the interporosity flow coefficient and permeability. This was done by minimizing the difference between the pressure derivatives obtained from simulations and experiments. Following this, the pressures were fitted to obtain the storativity ratio. It can be observed from Fig. 12 (a) that there is very good agreement between the simulation results and experimental results of Alnoaimi et al. (2016), indicating that the transient interporosity flow model is able to capture the flowback phenomenon after the upstream and downstream pressures converge. It can be observed from Fig. 12 (b) that there are only late-time pressure derivatives due to the lack of early-time data. The pressure derivative data points appear scattered due to small fluctuations in the pressure data. When the upstream and downstream pressures approach convergence, the pressure derivatives are very small, with a value less than 10^{-5}. The pressure noise is not negligible with respect to the pressure decay at $t_D > 100$,

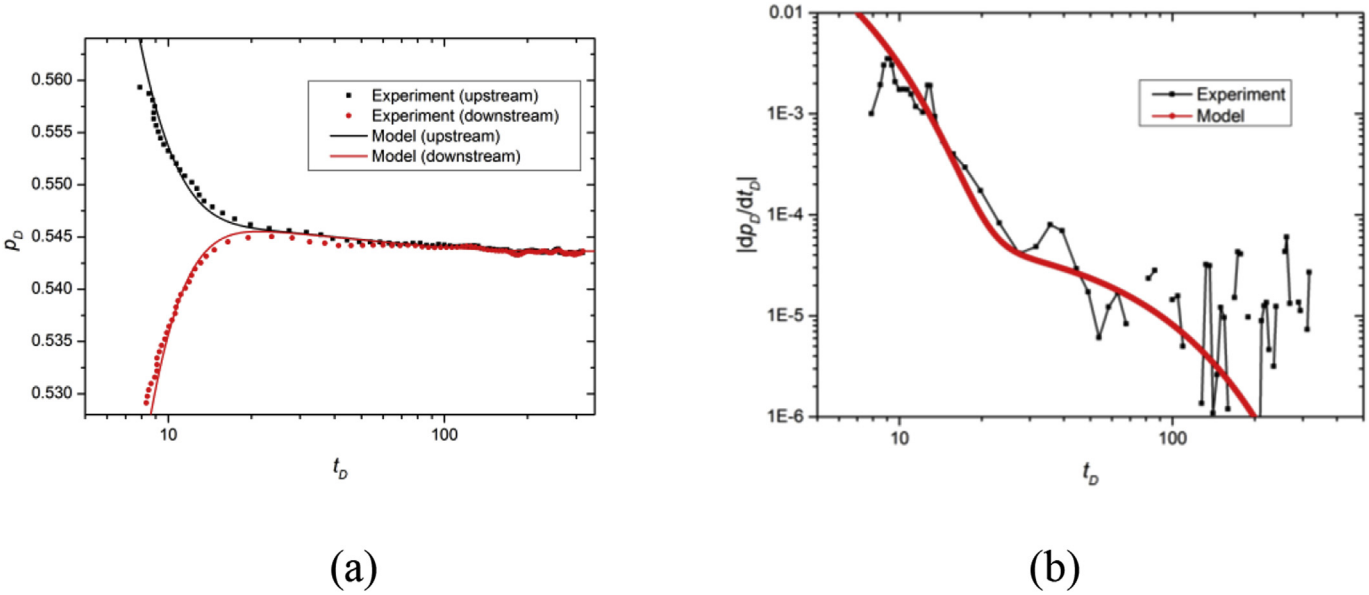

Fig. 12. Comparison between the simulation results and experimental data of Alnoaimi et al. (2016) for (a) pressure histories and (b) pressure derivative histories (from Alnoaimi et al., 2016, Fig. 7(c)).

resulting in fluctuations in the pressure derivatives. Hence, the pressure derivative values are not reliable at $t_D > 100$ and the data within this range cannot be used to verify the pressure derivative method. Overall, the fitting of the pressure derivatives is acceptable and it can be deduced that the transient dual-porosity model is suitable to assess the flow characteristics in Haynesville shale core, containing microcracks within a size range of 3.0–4.5 mm (Alnoaimi et al., 2016). This indicates that the transient dual-porosity model is able to capture the flow characteristics in cores with dense microcracks. The dual-porosity model is also able to capture the flow characteristics in cores with sparse microcracks, but further research is needed to verify the accuracy of the model.

These two experimental cases preliminarily verified the proposed method, and more experiments would be carried out in the future to further verify this method.

7. Conclusions

In this study, numerical simulations were conducted to analyze the results of pulse decay tests for dual-porosity media. Based on the results, homogeneous and dual-porosity media can be distinguished based on pressure curves because the pressures of dual-porosity media will decrease gradually to $A_d/(A_u + A_d + A_uA_d)$ after the upstream and downstream vessel pressures converge into a plateau. However, if the volumes of the upstream and downstream vessels are ten times larger than the pore volume, the permeability of the rock sample obtained from conventional semi-logarithmic linear analysis is almost equal to the permeability of the macropores (which is slightly influenced by the storativity ratio), and this makes it difficult to distinguish between homogeneous and dual-porosity media. Hence, the pressure derivative method was proposed in this work in order to distinguish between homogeneous and dual-porosity media. In general, both the pressure and pressure derivative curves should be used to determine the parameters (permeability, storativity ratio, and interporosity flow coefficient) of the dual-porosity models. The applicability of the pressure derivative method was verified by comparing the simulation results of the transient interporosity flow model with the experimental data of other researchers. The effects of the upstream and downstream vessel volumes, storativity ratio, and interporosity flow coefficient on the pressure derivative curves are summarized as follows:

(1) In order to distinguish dual-porosity media from homogeneous ones, the volumes of the upstream and downstream vessels should be within one-tenth to ten times the pore volume.
(2) The larger the storativity ratio, the faster the upstream pressure changes and the slower the downstream pressure changes. The height of the first pressure plateau decreases with an increase in the storativity ratio.
(3) The effect of the interporosity flow coefficient on the pressure derivative curves is more pronounced during the late stage. Hence, the characteristics of the transient and pseudosteady-state dual-porosity models can be distinguished based on the pressure derivative curves in the late stage.

Acknowledgments

The authors acknowledge the Key Laboratory for Mechanics in Fluid solid Coupling Systems, CAS and the National Natural Science Foundation of China (Grant No.11602276) for the financial support to this research.

Appendix A. Dual-porosity model

Figure A-1 shows the schematic of the dual-porosity model. The following assumptions were made for the analysis: (1) The testing fluid is single phase and slightly compressible; (2) The fluid compressibility and viscosity are constant; (3) The flow obeys the Darcy law with constant permeability, and the quadratic pressure gradient is negligible; (4) The pore compressibility and porosity are constant; (5) The temperature is constant throughout the experiment; (6) The upstream and downstream vessels are treated as isobaric bodies; (6) Gas leaks are negligible. According to the governing equations of pseudosteady-state dual-porosity model (Warren and Root, 1963), the one-dimensional governing equation for pulse decay test is given by:

$$\frac{\mu(c_t\phi)_f}{k_f}\frac{\partial p}{\partial t} = \frac{\partial^2 p}{\partial x^2} + \frac{\alpha k_m}{k_f}(p_m - p_f) \tag{A-1}$$

$$-\alpha k_m(p_m - p_f) = \mu(\phi c_t)_m\frac{\partial p_m}{\partial t} \tag{A-2}$$

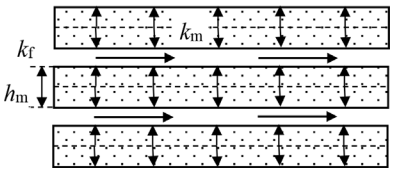

Fig. A1. Schematic of the dual-porosity model

Equation (A-1) represents the gas flow in the fracture whereas equation (A-2) represents the gas flow from the matrix to the fracture.

The initial conditions are:

$$p_f(x, 0) = p_m(x, 0) = p_d(0),\ 0 < x < L \tag{A-3}$$

The boundary conditions are:

$$p_f(0, t) = p_u(t),\ t \geq 0 \tag{A-4}$$

$$p_f(L, t) = p_d(t),\ t \geq 0 \tag{A-5}$$

$$\frac{dp_u}{dt} = \frac{k_f}{(c_g + c_{V_u})\mu\phi L}\frac{V_p}{V_u}\frac{\partial p_f}{\partial x}\bigg|_{x=0},\ t > 0 \tag{A-6}$$

$$\frac{dp_d}{dt} = \frac{-k_f}{(c_g + c_{Vd})\mu\phi L}\frac{V_p}{V_d}\frac{\partial p_f}{\partial x}\bigg|_{x=0}, \; t > 0 \tag{A-7}$$

Assuming that the core matrix is a slab, the governing equations of the transient dual-porosity model for the pulse decay test are (de Swaan, 1976):

$$\frac{(\phi c_t)_f \mu}{k_f}\frac{\partial p_f}{\partial t} = \frac{\partial}{\partial x}\left(\frac{\partial p_f}{\partial x}\right) + \frac{\mu}{k_f}q_m \tag{A-8}$$

$$\frac{(\phi c_t)_m \mu}{k_m}\frac{\partial p_m}{\partial t} = \frac{\partial^2 p_m}{\partial z^2} \tag{A-9}$$

$$q_m = \frac{2}{h_m}\frac{k_m}{\mu}\frac{\partial p_m}{\partial z}\bigg|_{z=0} \tag{A-10}$$

Equations (A-8) and (A-9) represent the flows in the fracture and matrix, respectively, whereas equation (A-10) represents the flow from the matrix to the fracture. In addition to the previous initial conditions ((A-3)) and boundary conditions ((A-4)–(A-7)), the transient dual-porosity model is subject to the following interfacial conditions:

$$\frac{\partial p_m}{\partial z}\bigg|_{z=h_m/2} = 0 \tag{A-11}$$

$$p_m|_{z=0} = p_f \tag{A-12}$$

Appendix B. Numerical solution for the pseudosteady-state dual-porosity model

The sample is assumed to be divided into N segments with a space interval of Δx_D and time interval of Δt_D. The finite difference schemes for equations (11) and (12) of the pseudosteady-state dual-porosity model are:

$$\frac{1}{\Delta x_D}\left(\frac{p_{fD,j+1}^{n+1} - p_{fD,j}^{n+1}}{\Delta x_D} - \frac{p_{fD,j}^{n+1} - p_{fD,j-1}^{n+1}}{\Delta x_D}\right) + \lambda_D\left(p_{mD,j}^{n+1} - p_{fD,j}^{n+1}\right) = \omega\frac{p_{fD,j}^{n+1} - p_{fD,j}^{n}}{\Delta t_D} \tag{B-1}$$

$$-\lambda_D\left(p_{mD,j}^{n+1} - p_{fD,j}^{n+1}\right) = (1-\omega)\frac{p_{mD,j}^{n+1} - p_{mD,j}^{n}}{\Delta t_D} \tag{B-2}$$

The finite difference schemes for the boundary conditions (equations (5) and (6)) are:

$$\frac{p_{fD,1}^{n+1} - p_{fD,0}^{n+1}}{\Delta x_D}A_u = \frac{p_{fD,0}^{n+1} - p_{fD,0}^{n}}{\Delta t_D} \tag{B-3}$$

$$-\frac{p_{fD,N}^{n+1} - p_{fD,N-1}^{n+1}}{\Delta x_D}A_d = \frac{p_{fD,N}^{n+1} - p_{fD,N}^{n}}{\Delta t_D} \tag{B-4}$$

Equations (B-1)–(B-4) can be simplified as:

$$-\lambda p_{fD,j+1}^{n+1} + (2\lambda + \omega + \lambda_D\Delta t_D)p_{fD,j}^{n+1} - \lambda p_{fD,j-1}^{n+1} - \lambda_D\Delta t_D p_{mD,j}^{n+1} = \omega p_{fD,j}^{n} \tag{B-5}$$

$$[\lambda_D\Delta t_D + (1-\omega)]p_{mD,j}^{n+1} - \lambda_D\Delta t_D p_{fD,j}^{n+1} = (1-\omega)p_{mD,j}^{n} \tag{B-6}$$

$$-\theta A_u p_{fD,1}^{n+1} + (\theta A_u + 1)p_{fD,0}^{n+1} = p_{fD,0}^{n} \tag{B-7}$$

$$(\theta A_d + 1)p_{D,N}^{n+1} - \theta A_d p_{D,N-1}^{n+1} = p_{D,N}^{n} \tag{B-8}$$

where the superscript n represents the nth time step and the subscript j represents the node number. Here, λ and θ are defined as:

$$\lambda = \frac{\Delta t_D}{\Delta x_D^2}, \; \theta = \frac{\Delta t_D}{\Delta x_D} \tag{B-9}$$

There are $2(N+1)$ dimensionless pressure variables at every time step. For $(N+1)$ nodes, there are $(N+1)$ equations (equation (B-6)) whereas for $(N-1)$ internal nodes, there are $(N-1)$ equations (equation (B-5)). Equations (B-7) and (B-8) are used for the upstream and downstream nodes, respectively. Therefore, there are $2(N+1)$ unknown variables and $2(N+1)$ equations, resulting in a matrix with a size of $2(N+1) \times 2(N+1)$. Gaussian elimination is used to solve the system of equations.

Appendix C. Numerical solution for the transient dual-porosity model

For the transient interporosity flow model, the sample is not only divided into N segments, but the semi-thickness of the slab matrix is also divided into M segments. The space interval, matrix space interval, and time interval are denoted as Δx_D, Δz_D, and Δt_D, respectively. The finite difference schemes for the dimensionless governing equations (equation (15) and (16)) of the transient dual-porosity model are:

$$\frac{1}{\Delta x_D}\left(\frac{p_{fD,j+1}^{n+1}-p_{fD,j}^{n+1}}{\Delta x_D}-\frac{p_{fD,j}^{n+1}-p_{fD,j-1}^{n+1}}{\Delta x_D}\right)+\frac{\lambda_D}{6}\frac{p_{mD,j(1)}^{n+1}-p_{mD,j(0)}^{n+1}}{\Delta z_D}=\omega\frac{p_{fD,j}^{n+1}-p_{fD,j}^{n}}{\Delta t_D} \tag{C-1}$$

$$\frac{1}{\Delta z_D}\left(\frac{p_{mD,j(k+1)}^{n+1}-p_{mD,j(k)}^{n+1}}{\Delta z_D}-\frac{p_{mD,j(k)}^{n+1}-p_{mD,j(k-1)}^{n+1}}{\Delta z_D}\right)=\frac{12(1-\omega)}{\lambda_D}\frac{p_{mD,j(k)}^{n+1}-p_{mD,j(k)}^{n}}{\Delta t_D} \tag{C-2}$$

The finite difference schemes of the interfacial conditions (equation (19) are (20)) are:

$$\frac{p_{mD,j(M)}^{n+1}-p_{mD,j(M-1)}^{n+1}}{\Delta z}=0 \tag{C-3}$$

$$p_{mD,j(0)}^{n+1}-p_{fD,j}^{n+1}=0 \tag{C-4}$$

Equations (C-1)–(C-4) can be simplified as:

$$-\lambda p_{fD,j+1}^{n+1}+\left(2\lambda+\frac{\lambda_D}{6}\theta_1+\omega\right)p_{fD,j}^{n+1}-\lambda p_{fD,j-1}^{n+1}-\frac{\lambda_D}{6}\theta_1 p_{mD,j(1)}^{n+1}=\omega p_{fD,j}^{n} \tag{C-5}$$

$$-\frac{\lambda_1\lambda_D}{12}p_{mD,j(k+1)}^{n+1}+\left(\frac{\lambda_1\lambda_D}{6}+1-\omega\right)p_{mD,j(k)}^{n+1}-\frac{\lambda_1\lambda_D}{12}p_{mD,j(k-1)}^{n+1}=(1-\omega)p_{mD,j(k)}^{n} \tag{C-6}$$

$$p_{mD,j(M)}^{n+1}-p_{mD,j(M-1)}^{n+1}=0 \tag{C-7}$$

$$p_{mD,j(0)}^{n+1}-p_{fD,j}^{n+1}=0 \tag{C-8}$$

where

$$\theta_1=\frac{\Delta t_D}{\Delta z_D},\ \lambda_1=\frac{\Delta t_D}{\Delta z_D^2} \tag{C-9}$$

There are $(N+1)\times(M+1)$ dimensionless pressure variables at every time step. For $(N+1)$ nodes, there are $(M-1)$ equations (equation (C-6)) and two interfacial conditions (equations (C-7) and (C-8)). Equation (C-5) is used for $(N-1)$ internal nodes. Equations (B-7) and (B-8) are used for the upstream and downstream nodes, respectively. Therefore, there are $(N+1)\times(M+1)$ unknown variables with the same number of equations, resulting in a matrix with a size of $[(N+1)\times(M+1)]\times[(N+1)\times(M+1)]$. Solving this matrix is time-consuming and therefore, the pressures of the fracture and matrix can be fixed alternately in one iterative step in order to save computational time. When the matrix pressures are fixed, equations (C-5), (B-7), and (B-8) constitute a tridiagonal matrix with a size of $(N+1)\times(N+1)$. When the fracture pressures are fixed, equations (C-6), (C-7), and (C-8) constitute a tridiagonal matrix with a size of $(M+1)\times(M+1)$. This reduces the size of the matrices. A tridiagonal matrix can be solved more efficiently by using the Thomas algorithm (Quarteroni et al., 2007).

Appendix. DSupplementary data

Supplementary data to this article can be found online at https://doi.org/10.1016/j.jngse.2018.09.006.

References

Alnoaimi, K.R., Duchateau, C., Kovscek, A.R., 2016. Characterization and measurement of multiscale gas transport in shale-core samples. SPE J. 21 (2), 573–588.

Alnoaimi, K.R., Kovscek, A.R., 2013. Experimental and Numerical Analysis of Gas Transport in Shale Including the Role of Sorption. Presented at the SPE Annual Technical Conference and Exhibition, New Orleans, Louisiana, 30 September-2 October.

Bajaalah, K.S., 2009. Determination of Matrix and Fracture Permeabilities in Whole Cores Using Pressure Pulse Decay. Master Dissertation. King Fahd University of Petroleum and Minerals, Dhahran.

Bourbie, T., Walls, J., 1982. Pulse decay permeability: analytical solution and experimental test. SPE J. 22 (5), 719–921.

Brace, W.F., Walsh, J.B., Frangos, W.T., 1968. Permeability of granite under high pressure. J. Geophys. Res. 73 (6), 2225–2236.

Chen, T., Stagg, P.W., 1984. Semilog analysis of the pulse decay technique of permeability measurement. SPE J. 24 (6), 639–642.

Civan, F., Rai, C.S., Sondergeld, C.H., 2011. Shale permeability determined by simultaneous analysis of multiple pressure-pulse measurements obtained under different conditions. In: Presented at the North American Unconventional Gas Conference and Exhibition, The Woodlands, Texas, 14-16 June.

Civan, F., Rai, C.S., Sondergeld, C.H., 2012. Determining shale permeability to gas by simultaneous analysis of various pressure tests. SPE J. 17 (17), 717–726.

Clarkson, C.R., Bustin, R.M., 1999. The effect of pore structure and gas pressure upon the transport properties of coal: a laboratory and modeling study. 2. Adsorption rate modeling. Fuel 78 (11), 1345–1362.

Cronin, M.B., 2014. Core-scale Heterogeneity and Dual-permeability Pore Structure in the Barnett Shale. The University of Texas at Austin, USA PhD thesis.

Cui, X., Bustion, A.M.M., Bustion, R.M., 2009. Measurements of gas permeability and diffusivity of tight reservoir rocks:different approaches and their applications. Geofluids 9 (3), 208–223.

de Swaan, O.A., 1976. Analytic solutions for determining naturally fractured reservoir properties by well testing. SPE J. 16 (3), 117–122.

Dehghanpour, H., Shirdel, M., 2011. A triple porosity model for shale gas reservoirs. In: Presented at the Canadian Unconventional Resources Conference, Calgary, Alberta, Canada, 15-17 November.

Dicker, A.I., Smits, R.M., 1988. A Practical approach for determining permeability from laboratory pressure-pulse decay measurements. In: Presented at the 1988 SPE International Meeting on Petroleum Engineering, Tianjin, China, 1-4 November.

Heller, R., Vermylen, J., Zoback, M., 2014. Experimental investigation of matrix permeability of gas shales. AAPG Bull. 98 (5), 975–995.

Hsieh, P.A., Tracy, J.V., Neuzil, C.E., Bredehoeft, J.D., Silliman, S.E., 1981. A transient laboratory method for determining the hydraulic properties of 'tight' rocks – I. Theory. Int. J. Rock Mech. Min. Sci. Geomech. Abstr. 18 (3), 245–252.

Hudson, J.D., 2011. Quad-porosity Model for Description of Transport in Shale-gas Reservoirs. University of Oklahoma, USA (Master thesis).

Jia, B., Tsau, J.S., Barati, R., 2017. Evaluation of core heterogeneity effect on pulse-decay experiment. In: Presented at the International Symposium of the Society of Core Analysts, Vienna, Austria, 27 August-1 September.

Jones, S.C., 1997. A technique for faster pulse-decay permeability measurements in tight rocks. SPE Form. Eval. 12 (1), 19–25.

Kamath, J., Boyer, R.E., Nakagawa, F.M., 1992. Characterization of core-scale heterogeneities using laboratory pressure transients. SPE Form. Eval. 7 (3), 219–227.

Kwan, M.Y., Okazawa, T., Fortier, R.A., 1988. Application of the pulse decay technique to the measurement of heavy oil core fluid mobilities and porosity. J. Can. Petrol. Technol. 27 (5), 92–98.

Liu, H., Lai, B., Chen, J., Georgi, D., 2016. Pressure pulse-decay tests in a dual-continuum medium: late-time behavior. J. Petrol. Sci. Eng. 147, 292–301.

Lorinczi, P., Burns, A.D., Lesnic, D., Fisher, Q.J., Crook, A.J., Grattoni, C., Rybalcenko, K., 2014. Direct and inverse methods for determining gas flow properties of shale. In: Presented at the SPE/EAGE European Unconventional Resources Conference and Exhibition, Vienna, Austria, 25-27 February.

Metwally, Y.M., Sondergeld, C.H., 2011. Measuring low permeabilities of gas-sands and

shales using a pressure transmission technique. Int. J. Rock Mech. Min. Sci. 48 (7), 1135–1144.
Neuzil, C.E., Cooley, C., Silliman, S.E., Breliman, S., Hsieh, P.A., 1981. A transient laboratory method for determining the hydraulic properties of 'tight' rocks – II. Application. Int. J. Rock Mech. Min. Sci. Geomech. Abstr. 18 (3), 253–258.
Ning, X., Fan, J., Holditch, S.A., Lee, W.J., 1993. The measurement of matrix and fracture properties in naturally fractured cores. In: Presented at the Low Permeability Reservoirs Symposium, Denver, Colorado, 26-28 April.
Pan, Z., Ma, Y., Connell, L.D., Down, D.I., Camilleri, M., 2015. Measuring anisotropic permeability using a cubic shale sample in a triaxial cell. J. Nat. Gas Sci. Eng. 26, 336–344.
Quarteroni, A., Sacco, R., Saleri, F., 2007. Numerical Mathematics, second ed. Springer, New York, pp. 93–96.
Walder, J., Nur, A., 1986. Permeability measurement by the pulse decay method: effects of poroelastic phenomena and nonlinear pore pressure diffusion. Int. J. Rock Mech. Min. Sci. Geomech. Abstr. 23 (3), 225–232.
Warren, J.E., Root, P.J., 1963. The behavior of naturally fractured reservoirs. SPE J. 3 (3), 245–255.
Yuan, W., Pan, Z., Li, X., Yang, Y., Zhao, C., Connell, L.D., Li, S., He, J., 2014. Experimental study and modelling of methane adsorption and diffusion in shale. Fuel 117, 509–519.